# Comparisons of Upper Tropospheric Humidity Retrievals from TOVS and METEOSAT

C. Escoffier,[1] J. Bates,[2] A. Chédin,[3] W. B. Rossow,[4] and J. Schmetz,[5]

[1]Goddard Institute for Space Studies, Columbia University, New York, NY, USA

[2]NOAA/ERL-R/ET1A, Environmental Technology Laboratory, Boulder, CO, USA

[3]Laboratoire de Météorologie Dynamique, LMD/ARA, Palaiseau, France

[4]NASA/Goddard Institute for Space Studies, New York, NY, USA

[5]EUMETSAT, Darmstadt, Germany

Short title: COMPARISONS OF UTH FROM TOVS AND METEOSAT

**Abstract.** Two different methods for retrieving Upper Tropospheric Humidities (UTH) from the TOVS (TIROS Operational Vertical Sounder) instruments aboard NOAA polar orbiting satellites are presented and compared. The first one, from the Environmental Technology Laboratory, computed by J. Bates and D. Jackson (hereafter BJ method), estimates UTH from a simplified radiative transfer analysis of the upper tropospheric infrared water vapor channel at wavelength measured by HIRS (6.3$\mu$m). The second one results from a neural network analysis of the TOVS (HIRS and MSU) data developed at the Laboratoire de Meteorologie Dynamique (hereafter the 3I (Improved Initialization Inversion) method). Although the two methods give very similar retrievals in temperate regions (30-60°N and S), an absolute bias up to 16% appears in the convective zone of the tropics. The two datasets have also been compared with UTH retrievals from infrared radiance measurements in the 6.3$\mu$m channel from the geostationary satellite METEOSAT (hereafter MET method). The METEOSAT retrievals are systematically drier than the TOVS-based results by an absolute bias between 5 and 25%. Despite the biases, the spatial and temporal correlations are very good. The purpose of this study is to explain the deviations observed between the three datasets. The sensitivity of UTH to air temperature and humidity profiles is analysed as are the clouds effects. Overall, the comparison of the three retrievals gives an assessement of the current uncertainties in water vapor amounts in the upper troposphere as determined from NOAA and METEOSAT satellites.

# 1. Introduction

One of the major controversies about the water vapor atmospheric distribution concerns its amount in the upper troposphere. Outgoing Long wave Radiation (OLR) fluxes are very sensitive to this quantity [*Spencer and Braswell,* 1997], especially in a dry atmosphere, so upper tropospheric humidity variations can have important effects on climate changes.

Unfortunately, water vapor is poorly measured particularly in the upper troposphere where radiosonde measurements are unreliable [*Elliott and Gaffen,* 1991; *Soden and Lanzante,* 1996]. Therefore, water vapor measured remotely from satellites is a way to add important information, especially since satellites provide the only global analysis of humidity fields possible. Recent studies have described several datasets of clear-sky radiances from the moisture-sensitive 6.7-$\mu$m channel onboard geostationary satellites [*Schmetz and Turpeinen,* 1988; *Turpeinen and Schmetz,* 1989; *Soden and Bretherton,* 1993] and from the moisture sensitive channels onboard polar orbiting satellites [*Bates et al.,* 1996; *Stephens et al.,* 1996; *Chaboureau et al.,* 1998]. Geostationary measurements provide information regarding the vertically averaged water vapor content of the upper troposphere (roughly 300-600mb). Polar orbiter measurements describe the vertical distribution of the tropospheric moisture from the surface to about 100hPa.

Several methods exist to retrieve water vapor amount in the upper troposphere from satellite infrared radiances. The different methods are usually dependent on ancillary data such as radiosondes or European Center for Medium-range Weather Forecasts

(ECMWF) forecast profiles. A comparison between different satellite retrievals is one way of validating the remote sensing observations. In this study, we compare three datasets of Upper Tropospheric Humidity (UTH) retrievals from satellites (described in section 2) in order to assess current uncertainties. Since we use the METEOSAT observations, the domain of study is restricted to the METEOSAT view of the Earth, centered at 0V, ,0N, with a 55° latitude-longitude radius. A physical retrieval method based on a neural network approach is compared to two analytical methods based upon a simplified radiative transfer theory to relate brigthness temperature to relative humidity. Retrievals from geostationary and from polar orbiting satellites are also compared. Perfect agreement is not expected as algorithms, spectral channels and the upper tropospheric layers observed are slightly different. The results of the comparisons are described in the third section. In the last section, we try to explain the systematic differences.

## 2. Data description

The quantity UTH (a simple interpretation of brightness temperature, $T_b$) is defined as the weighting-function-averaged relative humidity computed over a deep layer of the upper troposphere between 200 and 600hPa for both TIROS-N Operational Vertical Sounder (TOVS) channel 12 (6.3$\mu$m wavelength) and the METEOSAT water vapor channel, (6.7$\mu$m wavelength). Such channels are sensitive both to air temperature and moisture in the upper troposphere, which explains the interpretation of $T_b$ in term of relative humidity, which is a function of temperature and specific humidity. The

following study is done for four months in 1989 (January, April, July and October) in the METEOSAT domain. The METEOSAT image is subdivided into segments of 32 x 32 IR pixels, corresponding to about 160x160km at the subsatellite point and about 200x200km as a mean value. The other datasets used in this study are averaged on that grid. Twice daily retrievals are used to compute UTH from METEOSAT (11 AM and PM), whereas four retrievals, two from NOAA-10 (7.30 AM and PM) and two from NOAA-11 (2.30 AM and PM), are mixed to compute UTH in both TOVS datasets. The temporal resolutions examined are 5-days and monthly averages.

In the following, the three UTH datasets are defined and the relative humidity in percent is calculated with respect to liquid water. Percent values will also represent absolute differences of relative humidity or relative differences of relative humidity as precised in the text.

### 2.1. UTH from TOVS/HIRS: A simple $T_b$ interpretation

This first UTH dataset is from the Environmental Technology Laboratory and was computed by J. Bates and D. Jackson (BJ-UTH). The computation uses TOVS/HIRS (TIROS-N Operational Vertical Sounder/ High resolution Infrared Radiation Sounder) radiances from channels 12 (6.7$\mu$m), 4 (14.2$\mu$m) and 6 (13.7$\mu$m). Channels 4 and 6 are used for operational temperature sounding (respectively $T_4$ and $T_6$), whereas channel 12 is sensitive to water vapor and air temperature in upper troposphere. The radiances are limb corrected and cloud cleared by the operational NESDIS (National Environmental Satellite Data and Information Service) TOVS processing package

[*Werbowetzki*, 1981; *Kidwell*, 1991]. The UTH retrieval method is based on the work by *Soden and Bretherton* [1993], using forward radiative transfer simulation, with some changes according to *Stephens et al.* [1996]. The 6.7$\mu$m brightness temperature $T_b$ is interpreted as UTH, which is supposed to be the relative humidity in the 300-500hPa layer, following the equation:

$$log(\frac{< UTH >}{< \beta >}) = a + bT_b \tag{1}$$

where $< . >$ stands for the vertical average of the quantity. $< \beta >$ is a function of the difference ($T_6$-$T_4$) as shown in Fig.11 of *Stephens et al.* [1996], except that the factor cos$\theta$, is equal to 1, since angular corrections were applied to the radiance data.

Minor changes, such as using the profile information from the climatological data base TIGR-3 [*Chédin et al.*, 1985; *Chevallier et al.*, 1998] instead of TIGR-2, changing the Malkmus [*Malkmus*, 1967] radiative transfer model for the MODTRAN [*Berk et al.*, 1989] model, and basing weighting function on temperature profiles instead of atmospheric transmission (in order to allow the weighting function to stay in the upper troposphere for most profiles) have been introduced by *D. Jackson* (1999, personal communication). An uncertainty of approximately 15-20% (relative error) is estimated for UTH [*Stephens et al.*, 1996] but larger uncertainties exist poleward of 45°. This a limitation of the method, which has difficulty retrieving UTH when air temperature is two low.

The BJ-UTH values have been constrained in order to avoid relative humidities

with respect to ice greater than 100%, which leads the UTH values with respect to water (the BJ-UTH product) smaller than 70%, a threshold observed in the data (see section 3.).

## 2.2. UTH from METEOSAT: A simple $T_b$ interpretation

The radiances come from the water vapor (WV) channel of METEOSAT, sensitive to radiation between 5.7 and 7.1-$\mu$m. The METEOSAT UTH products (MET-UTH), provided by EUMETSAT are produced following *Schmetz and Turpeinen* [1988] method based on a look-up table derived from radiative transfer calculations for a set of fixed UTH. The ECMWF forecast temperature profiles (from surface to 100hPa) and ECMWF forecast humidity profiles (from surface to 600hPa) are used in the method as adequate knowledge of the atmospheric structure. Between 300-600hPa, the humidity profile is represented by the UTH and above 300hPa humidity decreases linearly to reach 0% at 100hPa. Spectral radiances are calculated with an efficient radiative transfer model [*Schmetz,* 1986]. These calculations give a two entry-table (UTH and $T_b$ from WV channel). The absolute error on UTH is estimated at 10-15% [*Schmetz and Turpeinen,* 1988]. For the 1989 products, UTH was derived only for areas completly free of clouds at pressure level below 700hPa.

Since no calibration of the water vapor channel is performed aboard the satellite, a calibration method is implemented. Temperature and humidity profiles from radiosondes are used with the radiative transfer model to simulate radiances. The simulated radiances are compared to the 6.3$\mu$m channel radiances in order to calculate

a calibration coefficient [*Schmetz and Turpeinen,* 1988]. The quality of the calibration coefficient is monitored by following the bias between the UTH (obtained from the look-up table) and in-situ humidities from radiosondes. MET-UTH products used in this study are from the year 1989. Radiances for January and April come from METEOSAT-3, while radiances for July and October come from MET-4. The calibration described above has been applied to the radiances used to calculate the UTH-MET product of 1989.

Note that a new calibration described in *van de Berg et al.* [1995] tends to decrease the radiances by a 8% relative bias (and so increase UTH by a 20% relative bias) but it has not been applied yet to the UTH products of 1989.

### 2.3. UTH from TOVS/HIRS: A neural network approach

UTH is computed from the precipitable water amount in the 300-500hPa layer retrieved with the Improved Initialization Inversion (3I) method [*Chédin et al.,* 1985; *Scott et al.,* 1999] applied to NOAA-TOVS radiances (hereafter called 3I-UTH). This water vapor dataset is provided by the LMD. As for the BJ-UTH, the level 1B satellite radiance data are calibrated using coefficients provided by NOAA following the procedures set forth in [*Kidwell,* 1991]. The 3I method, dedicated to retrieve atmospheric, cloud, and surface variables, is a physico-statistical method based on a pattern recognition approach. After the determination of the temperature profile, cloud amount along with cloud top pressure and temperature are estimated using the procedure described by *Wahiche et al.*[1986] and improved by *Stubenrauch et al.* [1996]

and *Stubenrauch et al.* [1999]. The HIRS radiances in channels sensitive to water vapor, HIRS 8(11.1$\mu$m), 10(8.3$\mu$m), 11(7.3$\mu$m) and 12(6.7$\mu$m) and in the window channels are then corrected for the effects of partial cloud cover, making use of the previously determined cloud parameters. No cloud correction is attempted if the effective cloud amount is larger than 60%. Precipitable water amounts (above the surface to 100hPa and above the 850, 700, 500 and 300hPa levels to 100hPa) are then retrieved using a non-linear neural network approach [*Chaboureau et al.*, 1998]. The neural network is trained using the atmospheric profiles from the TIGR-3 data base as outputs and the corresponding radiances calculated from the "4A" (Automatized Atmospheric Absorption Atlas [*Scott et al.*, 1981]) model as inputs.

To be compared with MET-UTH or BJ-UTH products, the 3I precipitable water amount in the 300-500hPa layer has to be transformed into UTH. As the transformation is strongly sensitive to air temperature (see section 4.2), the 3I-UTH has been calculated using daily retrieved precipitable water amount and temperature of the 300-500hPa layer and then 5-day or monthly averaged. Moreover, the saturated vapor pressure, dependent also on air temperature, has been calculated with respect to liquid water at three levels within the 300-500hPa layer to have more accurate UTH results (UTH is not exactly uniform in the 300-500hPa layer).

# 3. Results

## 3.1. Spatial Variability

Figure 1 presents scatter plots in the tropical portion of the METEOSAT view that compare the three UTH datasets. It is obvious that 3I-UTH is the more humid for tropical regions (a slope of 1.3 exists compared with BJ-UTH and of 1.7 compared with MET-UTH) and MET-UTH is the driest (the slope of BJ-UTH in function of MET-UTH is 1.23). The larger dynamical range for the 3I-UTH results from a much better agreement in the dry regions than in humid regions. Despite the biases observed, the three datasets show similar spatial patterns. Indeed, the spatial correlations are larger than 0.95 with an absolute standard deviation smaller than 6.5%. Two out of the four months in Table 1 (January and April) show smaller correlation in the comparison with METEOSAT (0.92-0.94) and greater absolute standard deviation of about 5 to 7%. We cannot confirm that the same method has been applied to MET-3 (January/April) and MET-4 (July/October).

Figure 1

Table 1

In temperate regions (30-60°N and S), the correlation are always larger than 0.98 with an absolute standard deviation smaller than 3.5% as shown in Table 2, except for the comparisons with BJ-UTH where correlation is around 0.95 (in January and July) with an absolute standard deviation larger than 4.4%. This discrepancy between BJ-UTH and the two other datasets, also observed on the scatter plots of Figure 2, appears mostly for the highest latitudes in winter (north hemisphere in January and south hemisphere in July), where BJ-UTH becomes larger than the two other

Table 2

datasets. The limits of the BJ method to retrieve UTH when air temperatures are low has been stressed in the description of this method. BJ-UTH and 3I-UTH have the best agreement, 3I-UTH being a little larger between 30-40° (N and S) and BJ-UTH larger between 40-60° (N and S). MET-UTH is always much smaller than both TOVS retrievals, the slope is between 1.76 and 1.80.

Figure 3, which illustrates the spatial differences between each dataset and the mean of the three, summarizes the spatial comparison (only July is shown). Each UTH dataset is in agreement with the mean to within 7% (absolute difference) in the dry regions and within 21% (absolute difference) in the more humid regions, UTH-3I being wetter and MET-UTH drier. The BJ-UTH is in agreement within 7% (absolute difference) over the whole region, except in the winter highest latitudes where it is more humid by up to 20%. A 7% absolute bias in dry regions and a 21% absolute bias in humid regions represents a relative bias to the mean of about 30% in both regions.

Figure 3

In conclusion, the three datasets, are very well correlated spatially but systematic discrepancies exist in the magnitude of the mean variation from humid to dry conditions. Indeed, the quantitative agreement is still a relative bias to the 3 datasets mean of 30%, despite the fact that the accuracy of each dataset has been estimated to be about 10 to 20% (relative error).

The best spatial correlation for the four months is observed between BJ and 3I in tropical regions and between MET and 3I in midlatitudes. The best relative humidity amount agreement is observed between BJ and MET in tropical regions and between 3I and BJ in midlatitudes. Since the spatial correlation is rather good, it is worth looking

more carefully at the temporal variability, using monthly and 5-day-mean.

### 3.2. Temporal Variability

Variations on two time scales are explored. Figure 4 shows the monthly differences of zonal mean (every 5° longitude) UTH between summer and winter months and between autumn and spring months, approximating the annual cycle amplitude in the 3 datasets. The METEOSAT view is divided into two parts, the west part being dominated by ocean (Figure 4 left) and the east part by land (Figure 4 right). Error bars represent the zonal mean standard deviation for the 3I dataset (which has the largest variability). The January-July difference is significant over land, showing the seasonal movement of the Inter Tropical Convergence Zone (ITCZ) accross the equator. While on the sea (Figure 4 left), the January-July difference is not significant compared to the error bars. The ITCZ has less variability over sea than over land as also shown by precipitation analyses and water vapor data in *Peixoto and Oort* [1992].

Figure 4

The April-October difference has a significant positive maximum in the southern tropical ocean (West part), which is not observed on land, linked to a large relative humidity and precipitation rate east of Brazil over the southern Atlantic ocean in April.

In general, the zonal mean correlation between the three datasets is good. 3I presents slightly larger amplitude but not significantly, compared to the error bar. The annual amplitudes given by the three datasets are similar.

In the second study, we select four regions of 15° latitude by 15° longitude on the

METEOSAT view as shown on Figure 5. Regions A and B are in the tropical zone (15°N-15°S). A is definitely in a subsidence region while B has its relative humidity amount varying with ITCZ movement. The regions C and D are located northward and centered at latitudes 22.5°N (C) and 37.5°N (D). We focus on 5-day-average anomaly time series plotted in Figure 6. The anomalies are defined as 5-day average minus the mean for the corresponding month. The anomaly calculation eliminates the biases between the three datasets. In region A, the 5-day average correlation is very good (Table 3). In region B, 3I-UTH has significantly larger anomalies in April and January but is still correlated with the two other datasets (Figure 6). In the northern region D where the variations are smaller, the correlation is the worse but still good (0.6-0.7) as shown in Table 3. The error bars represent the spatial standard deviation to the mean. The rms between datasets varies from 5% (absolute deviation) between BJ-UTH and MET-UTH in dry tropical region A to 23% (absolute deviation) between 3I-UTH and MET-UTH in humid tropical region B (Table 3). Despite that large bias differences, the temporal variation of the three datasets are in agreement within the error bars, in the four regions. Thus, the anomalies determined from all three datasets appear to be reliable.

Figure 5

Figure 6

Table 3

Figure 7 is a space-time Taylor diagram which summarizes the spatial-temporal agreement between the three datasets. MET-UTH, which has the smallest average amount, has been chosen as the reference dataset. The circle identified by 1 is the normalized standard deviation for the reference dataset. The data plotted near that circle have similar amplitude variation as the reference data, the data closer to the

Figure 7

center have larger amplitude and the closer to the exterior circle have smaller amplitude variation than the reference dataset. The angle with respect to two horizontal axis represents the correlation with the reference dataset. High correlations are closer to the X-axis and low correlations closer to the Y-axis. 5-day-average time series for the four regions are represented as well as for whole METEOSAT view. 3I-UTH has the largest space-time variance, except in region D where BJ-UTH has slightly greater amplitude. MET-UTH has the smallest variance, except in the subsidence region A where BJ-UTH show lower variance. A decrease of the space-time correlation with latitude is observed (Figure 7). In tropical regions, the correlation is between 0.87-0.94, in region C between 0.77-0.87 and smaller than 0.64 in region D. A global correlation of about 0.8 is found for the whole METEOSAT view.

## 4. Can the bias between the three datasets be explained?

According to the results of section 3, a disagreement is observed on the relative humidity amount and on the time-space variance. In the present section, we try to explain the cause of these discrepancies.

### 4.1. Weighting function

3I-UTH provides values larger than the two other datasets in the convective zones, but similar in subsidence zones. 3I-UTH values are for the layer 300-500hPa whatever the region observed and its conditions, whereas the precise layer represented by the two other methods depends on the water vapor weighting function, which depends on the

water vapor amount and vertical profile. The maximum of the weighting function shifts from about 300hPa for a wet tropical profile to about 500hPa for a dry tropical profile (Figure 8). The maximum of the weighting function also depends on the view angle of the satellite. In humid cases, the BJ and MET methods measure UTH in a layer slightly above 300-500hPa and lower in dry cases. The relative humidity amount measures by these two methods is different than by the 3I method, depending on the profile. The effect of the shifting weighting function is to reduce the magnitude of the difference of UTH between wetter and drier profiles, which explains the larger dynamical range of 3I-UTH. The so-called UTH is not exactly the relative humidity of the 300-500hPa layer measured by the 3I method as it depends on the shift of the weighting function peak.

Figure 8

Using the 4A radiative transfer model, we calculated the brightness temperatures corresponding to all the TIGR-3 profiles for the four following water vapor channels: channel 12 (centered in 6.7$\mu$m) for HIRS on NOAA-10 and NOAA-11 and the water vapor channel (centered in 6.3$\mu$m) for MET-3 and MET-4. Two examples are plotted on Figure 8, one for a dry profile and one for an humid profile. Although the instrument spectral response function shapes are very different, the weighting functions plotted on Figure 8 are nearly the same, but the same water vapor amounts correspond to different brightness temperatures. The bias between brightness temperatures from MET-3 and MET-4 is about 3°K. The absolute difference between METEOSAT and NOAA-TOVS brightness temperature is about 1.5°K. These brightness temperature discrepancies are observed for all the TIGR-3 profiles. To obtain UTH, a calibration treatment is applied on radiances at the EUMETSAT european operational center and the UTH algorithm

is adjusted to each satellite to compensate for the brightness temperature discrepancies. Thus, UTH from MET-3 and MET-4 in the present study are not so different.

### 4.2. Air temperature sensitivity of the transformation from precipitable water amount to relative humidity

To illustrate the sensitivity of UTH to air temperature, we made three experiments on the transformation of the 3I precipitable water amount into relative humidity.

In the first experiment, the 3I precipitable water amount is transformed into UTH using 3I retrieved air temperature ($UTH_t$) and this value +1°K ($UTH_{t+1}$). The 1°K difference, which corresponds to a 0.5% relative error in air temperature, introduces more than 10% relative error in UTH (not shown). This result is in agreement with *Peixoto and Oort* [1996] who shows that 1% variation on air temperature can induce more than 20% relative error in UTH.

The sensitivity of the transformation to air temperature errors is emphasized in a second experiment, which consists in comparing two 3I-UTH products: the first product ($UTH_d$) is transformed from daily precipitable water amount and daily air temperature, then averaged over the month. The second product ($UTH_m$) is transformed using the monthly mean values of precipitable water amount and air temperature. Table 4 shows the difference between these two products. $UTH_m$ is systematically larger than $UTH_d$ by an absolute bias of 4% due to the transformation sensitivity to air temperature. This effect results from the fact that the monthly average air temperature is less variable by about 0.5% compared to daily air temperature and in this way produces the 4%

absolute difference on UTH.

The last sensitivity test to air temperature is done by using two different saturated vapor pressures. Air temperature averaged over the 300-500hPa layer is used to calculate the first saturated vapor pressure ($ew_1$). Air temperatures derived at three different levels (300, 400 and 500hPa) give three saturated vapor pressures, which are then averaged over the whole layer ($ew_3$). The UTH dataset calculated with $ew_3$ is systematically drier than the UTH dataset calculated with $ew_1$. The largest absolute bias, between 12 and 20%, is observed in the regions poleward of 40°, where the temperature is the coldest and UTH more sensitive to temperature variations. In the tropical band between 30°N and 30°S, the absolute bias is smaller than 6%, even smaller than 3% in the driest regions. The variability of temperature in the tropical band is relatively small. In January and July, a bias between 3 and 6% is obtained in the most humid regions.

The tests applied to 3I-UTH show that a 1% relative error of air temperature can induce more than 10% relative error of UTH. Likewise, a small variation of air temperature within the 300-500hPa layer can induce significant change in saturated vapor pressure and so in the UTH retrieval. The third test stresses the sensitivity in very low temperatures cases as the largest absolute biases are observed at high latitudes.

### 4.3. Cloudy Regions and Calibration in MET-UTH algorithm.

As shown in *Gaffen and Elliott* [1993], climatological column water vapor content of lower troposphere (surface to 400hPa) for clear skies is significantly lower than for

cloudy skies. The underestimate is about 10 to 15% in tropical regions and can be larger in midlatitude zones. An explanation for MET-UTH products providing values smaller than the two TOVS datasets (by a slope of 1.23 compared with BJ-UTH and by 1.7 compared to 3I-UTH) can be based on cloud effects. Indeed, in 1989, the MET operational product was derived only for areas of 32x 32 pixels, free of cloud at pressure level below 700hPa. In this way, even the clear radiances for such areas were not used to derive UTH. Obviously, this makes the product a lot drier since we avoid cloud free areas in the proximity of clouds and reduces also the dynamic range of MET-UTH product. A later change (after 1989) in the MET-UTH products include clear radiances from partly cloudy regions and led to a large increase in the dynamic range as shown in the following comparison. Figure 5 of *van de Berg et al.* [1991], before the change compared to Figure 5 of *Schmetz et al.* [1995], after the change exhibit a 20% absolute difference in the convective zone. So an absolute bias of 20% in moist regions can be explained by not including clear radiances from partly cloudy regions in MET method.

Another solution to decrease the bias found in the present study between NOAA-TOVS and MET UTH is to add *van de Berg et al.* [1995] calibration, which could decrease the radiances by a 8% relative bias and so increase MET-UTH by a 20% relative bias.

MET-UTH algorithm has been improved with years. And so, from 1982 to now, UTH products are not homogeneous. An update of all UTH product with the latest algorithm is planned at the EUropean organisation for the exploitation of METeorological SATellites (EUMETSAT).

## 5. Conclusion

In the present study, three upper tropospheric humidity (UTH) datasets retrieved from satellite measurements have been compared. The analyses are deceptively simple since the retrievals characteristics depend on the satellite radiances calibration, the retrieval algorithms, and all additional assumptions, particularly regarding the constancy of the vertical profiles of temperature and humidity.

The comparison of each dataset to the mean of the three gives an absolute bias of 20% in convective zone and of 7% in arid zones. Such a bias is significant (relative bias of 30%) compared to the uncertainty given on the UTH retrievals (estimated relative uncertainties of 10-20%). Different explanations for the discrepancies were investigated.

We note the difference between the UTH quantity and the relative humidity in the 300-500hPa layer. By definition, UTH is related to the 6.7$\mu$m brightness temperature interpreted in terms of the relative humidity in a broad layer (about 200-500hPa), but the precise limits of the layer represented vary depending on the air temperature, the specific humidity profile and the view angle of the satellite as we have shown. In other words, there is a systematic shift in the layer altitude with humidity. In contrast, the 3I method retrieves the relative humidity in a fixed layer, 300-500hPa, which is not exactly what is called UTH. The difficulty to compute UTH from precipitable water vapor content has been underlined and is mainly due to the transformation sensitivity to air temperature. The absence of using MET radiances in partly cloudy areas can also make an absolute difference between NOAA-TOVS and MET UTH retrievals up to 20%.

The three methods described in section 2 also use ancillary data to validate the model and to follow evolution of the sensor throughout its life time. Given the inaccuracy of the radiosonde observations of humidity in the upper troposphere [*Elliott and Gaffen*, 1991; *Soden and Lanzante*, 1996], reliance on them may introduce problems. Several studies [*Eyre*, 1987; *Reuter et al.*, 1988] also illustrate the impacts that ancillary data, like radiosonde observations, can have on the final retrievals. The errors introduced in this way in the three methods are hard to quantify. The MET method also requires a calibration of the radiances, not performed aboard the satellite.

On the other hand, the spatial and temporal correlation between the three methods is excellent, around 0.9 for the spatial correlation and 0.8 for the time-space correlation. 3I-UTH shows larger variability than the two other datasets; the lower variability of MET-UTH and BJ-UTH can come from the variation of the weighting function peak altitude with the upper troposphere humidity (section 4.1).

The present comparison gives an assessement of the uncertainty of relative humidity in the upper troposphere retrieved by satellite. An important relative bias of 30% exists among the datasets which is largely explained by measurement differences. A high correlation (larger than 0.8) both in space and time gives confidence in the UTH variability results. This study also underlines the importance of the details of each method for computing UTH. For this reason, additional work is needed to understand the relative merits of each method and the use of a consensus algorithm should be considered.

**Acknowledgment.** This work was funded by NASA as an augmentation to the NOAA/NASA Enhanced Data Sets Program, and as a contribution to the international WCRP's GEWEX.

# References

Bates, J., X. Wu, and D. Jackson, Interannual variability of upper-troposphere water vapor band brightness temperature, *J. Climate, 9,* 427-438, 1996.

Berk, A., L. Bernstein, and D. Robertson, Modtran: A moderate resolution model for lowtran 7, *Gl-tr-89-0122,* available from Spectral Sciences, Inc., Burlington, Mass., 1989.

Chaboureau, J. P., A. Chédin, and N. Scott, Remote sensing of the vertical distribution of atmospheric water vapor from the TOVS observations: Method and validation, *J. Geophys. Res., 103 (D8),* 8743-8752, 1998.

Chédin, A., N. Scott, C. Wahiche, and P. Moulinier, The improved initialization inversion method: A high resolution physical method for temperature retrievals from the TIROS-N series, *J. Clim. Appl. Meteorol., 24,* 124-143, 1985.

Chevallier, F., F. Cheruy, N. A. Scott, and A. Chédin, A neural network approach for fast and accurate computation of a longwave radiative budget, *J. Appl. Meteor., 37,* 1385-1397, 1998.

Elliott, W., and D. Gaffen, On the utility of radiosonde humidity archives for climate studies, *Bull. Am. Meteorol. Soc., 72,* 1507-1520, 1991.

Eyre, J., On systematic errors in satellite sounding products and their climatological mean values, /qjrms *113,* 279-292, 1987.

Gaffen, D. J., and W. P. Elliott, Column Water Vapor Content in Clear and Cloudy Skies, *J. Climate, 6,* 2278-2287, 1993.

Kidwell, K. B. *NOAA polar orbiter data user's guide,* 1991.

Malkmus, W., Random Lorentz model with exponential-tailed $s^{-1}$ line intensity distribution function, *J. Opt. Soc. Amer., 57,* 323-329, 1967.

Peixoto, J., and A. Oort *Physics of Climate*, 520pp., American Institute of Physics, 1992.

Peixoto, J., and A. Oort, The climatology of relative humidity in the atmosphere, *J. Climate, 9*, 3443-3463, 1996.

Reuter, D., J. Susskind, and A. Pursch, First-guess dependence of a physically based set of temperature-humidity retrievals from HIRS2/MSU data, *J. Atmos. Ocean. Technol., 5*, 70-83, 1988.

Schmetz, J., An atmospheric-correction scheme for operational application to METEOSAT infrared measurements, *ESA Journal, 10*, 145-159, 1986.

Schmetz, J., and O. Turpeinen, Estimation of the upper tropospheric relative humidity field from METEOSAT water vapor image data, *J. Appl. Meteorol., 27*, 889-899, 1988.

Schmetz, J., C. Geijo, W. Menzel, K. Strabala, L. van de Berg, K. Holmlund, and S. Tjemkes, Satellite observations of upper tropospheric relative humidity, clouds and wind field divergence, *Beitr. Phys. Atmosph., 68(4)*, 345-357, 1995.

Scott, N., and A. Chédin, A fast line method for atmospheric absorption computations: the automatized atmospheric absorption atlas, *J. Appl. Meteorol., 20*, 802-812, 1981.

Scott, N., A. Chédin, R. Armante, J. Francis, C. Stubenrauch, J.-P. Chaboureau, F. Chevallier and F. Cheruy, Characteristics of the TOVS pathfinder path-b data set, *Bull. Am. Meteorol. Soc., 80*, 2679-2701, 1999.

Soden, B., and F. Bretherton, Upper tropospheric relative humidity from GOES 6.7$\mu$m channel: Method and climatology for july 1987, *J. Geophys. Res., 98(D9)*, 16669-16688, 1993.

Soden, B., and J. Lanzante, An assessement of satellite and radiosonde climatologies of upper tropospheric water vapor, *J. Climate, 9*, 1235-1250, 1996.

Spencer, R., and W. Braswell, How dry is the tropical free troposphere? Implications for global warming theory, *Bull. Am. Meteorol. Soc., 78(6)*, 1097-1106, 1997.

Stephens, G., D. Jackson, and L. Wittmeyer, Global observations of upper-tropospheric water vapor derived from TOVS radiance data, *J. Climate, 9*, 305-326, 1996.

Stubenrauch, C., N. Scott, and A. Chédin, Cloud field identification for earth radiation budget studies: I) cloud field classification using HIRS/TOVS sounder measurements, *J. Appl. Meteor., 35(3)*, 416-427, 1996.

Stubenrauch, C., A. Chédin, R. Armante, and N. Scott, Clouds as seen by satellite sounders (3I) and imagers (ISCCP): Part II) a new approach for cloud parameter determination in the 3I algorithms, *J. Climate, 12*, 2214-2223, 1999.

Turpeinen, O., and J. Schmetz, Validation of the upper tropospheric relative humidity determined from METEOSAT data, *J. Atmos. Ocean. Tech., 6(2)*, 359-364, 1989.

van de Berg, L., A. Pyomjamsri, and J. Schmetz, Monthly mean upper tropospheric humidities in cloud-free areas from METEOSAT observations, *Int. Journal of Clim., 11*, 819-826, 1991.

van de Berg, L., J. Schmetz, and J. Whitlock, On the calibration of the METEOSAT water vapor channel, *J. Geophys. Res., 100(D10)*, 21069-21076, 1995.

Wahiche, C., N. A. Scott, and A. Chédin, Cloud detection and cloud parameters retrieval from the satellites of the TIROS-N series, *Ann. Geophys., 4(B2)*, 207-220, 1986.

Werbowetzki, A., Atmospheric sounding user's guide, *NOAA Tech. Rep. NESS 83.*, 1981.

---

J.Bates, NOAA/ERL-R/ET1A, Environmental Technology Laboratory, 325 Broadway, Boulder, CO 80303, USA. (e-mail: jbates@etl.noaa.gov)

A. Chédin, Laboratoire de Météorologie Dynamique, Analyse du Rayonnement Atmosphérique, Ecole Polytechnique, 91128 Palaiseau Cedex, France. (e-mail: chedin@jungle.polytechnique.fr)

C. Escoffier, Goddard Institute for Space Studies, Columbia University, 2880 Broadway 316A, New York, NY 10025, USA. (e-mail: christel@giss.nasa.gov)

W. B. Rossow, NASA/Goddard Institute for Space Studies, 2880 Broadway, New York, NY 10025, USA. (e-mail: wrossow@giss.nasa.gov)

J. Schmetz, EUMETSAT, Am Kavalleriesand 31, 64295 Darmstadt, Germany. (e-mail: Schmetz@eumetsat.de)

Received _____

To appear in the water vapor in climate special issue of *Journal of Geophysical Research*, 2001.

FIGURE CAPTIONS:

**Figure 1.** Scatter plots in the tropical regions (30°N-30°S) of METEOSAT view for January, April, July and October (4 months on the same plot). a: 3I versus BJ; b: 3I versus MET and c: BJ versus MET. In the legend. c stands for correlation and std for standard deviation.

**Figure 2.** Same as Figure 1 in the midlatitude regions (30-60°N and 30-60°S).

**Figure 3.** UTH difference (in %) between the datasets (a- 3I; b- BJ; c-MET) and the mean of the three in July. For clarity, note that light gray is between +21 and +7%; gray is between +7 and -7% and black between -7 and 21%. d: Average of the three datasets in July 1989 (in %).

**Figure 4.** Monthly differences of UTH zonal mean (average on every 5° of longitude over the West part (left) and the East part (right) of the METEOSAT view). January-July difference is represented in a and b; April-October difference in c and d. Negative latitude are for southern hemisphere. The standard deviation to the zonal mean (error bar) are shown for 3I only. -3I (full line); BJ-(dotted line) and -MET (dashed dashed).

**Figure 5.** Position of the four selected regions [15° latitude x 15° longitude]. A is centered with a cross; B with a star; C with a diamond and D with a triangle.

**Figure 6.** 5-day-average anomalies time series plotted for the four selected regions of Figure 5. -3I (full line); -BJ (dotted line); -MET (dashed line).

**Figure 7.** Taylor diagram: Space-Time variance of UTH in four regions and the global METEOSAT view by BJ and 3I with MET as reference. The radial coordinate gives the magnitude of total variance normalized to the reference dataset, and the polar coordinate gives the correlation with the reference dataset.

**Figure 8.** Water vapor channel's weighting function of four satellites (MET-3; MET-4; NOAA-10 and NOAA-11) for 2 profiles: on the left, an humid profile (300-500hPa humidity of 100%, 300-500hPa water vapor content of 1.26cm, air temperature between 246 and 270°K) and on the right, a dry profile (300-500hPa humidity of 1%, 300-500hPa water vapor content of 0.0064cm, air temperature between 235 and 263°K). In the legend, corresponding brightness temperatures follow the name of the satellite.

**Table 1.** Correlation and Standard Deviation (in %, in Parenthesis) for the 4 Months of each Scatter Plot of Figure 1 in the 30°S-30°N band of the METEOSAT View. Each Column represents a two datasets comparison (2600 Values).

| Months | 3I/BJ | 3I/MET | BJ/MET |
|---|---|---|---|
| January | 0.97(4.8) | 0.93(7.5) | 0.92(6.4) |
| April | 0.98(3.9) | 0.94(6.6) | 0.94(5.1) |
| July | 0.97(4.7) | 0.97(4.8) | 0.97(3.3) |
| October | 0.97(4.7) | 0.97(5.2) | 0.96(4.3) |

**Table 2.** Same as Table 1 in the 30-60°N and S band, corresponding to Figure 2 (900 Values).

| Months | 3I/BJ | 3I/MET | BJ/MET |
|---|---|---|---|
| January | 0.95(4.6) | 0.98(3.0) | 0.96(4.4) |
| April | 0.98(3.2) | 0.98(3.4) | 0.98(3.1) |
| July | 0.95(4.4) | 0.99(2.2) | 0.95(4.9) |
| October | 0.99(2.4) | 0.99(2.8) | 0.98(3.3) |

**Table 3.** Correlation and Rms (in %, in Parenthesis) in the 4 Different Regions Shown on Figure 5. The Correlation and Rms are Calculated with 5-Day Averaged Time Series (Plotted on Figure 6) over the Following Months: January, April, July and October 1989. Each Column Represents a two Datasets Comparison (20 Values).

| regions | 3I/BJ | 3I/MET | BJ/MET |
|---|---|---|---|
| A | 0.96(6.0) | 0.93(9.7) | 0.96(5.0) |
| B | 0.95(15.6) | 0.96(23.6) | 0.96(9.1) |
| C | 0.90(6.8) | 0.90(15.7) | 0.87 (9.6) |
| D | 0.76(5.9) | 0.62(17.7) | 0.78(16.8) |

**Table 4.** Absolute Rms and Bias ($UTH_m$-$UTH_d$) for four Months of 1989. $UTH_m$ Stands for 3I Relative Humidity Computed with Water Vapor Content and Air Temperature Monthly Means and $UTH_d$ for 3I Relative Humidity Computed with Daily Values and Monthly Averaged Afterward. The Region is only the Meteosat View.

| Months | January | April | July | October |
|---|---|---|---|---|
| Rms | 4.0 | 5.5 | 4.3 | 4.7 |
| Bias | -3.2 | -4.7 | -2.8 | -3.7 |

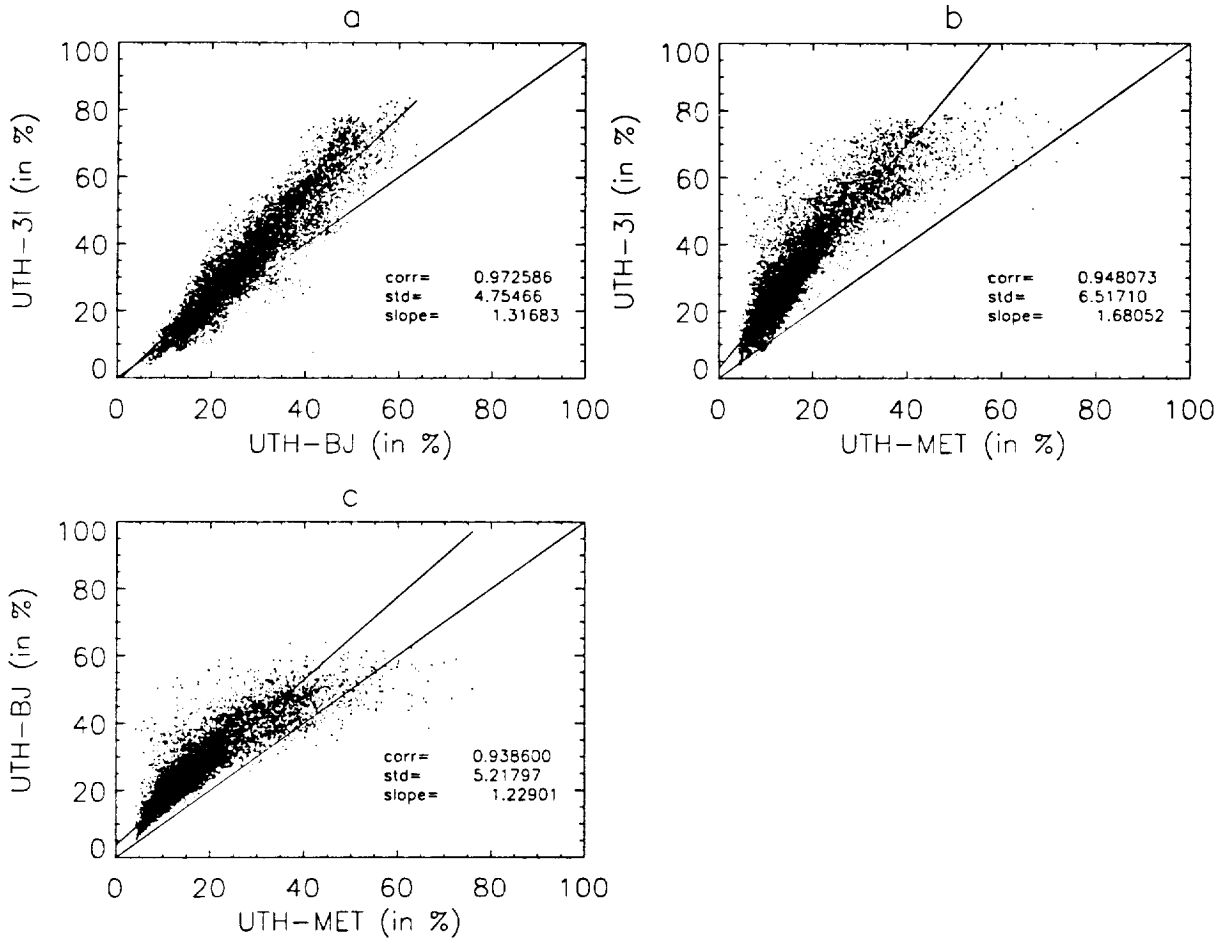


Figure 1: Scatter plots in the tropical regions (30°N-30°S) of METEOSAT view for January, April, July and October (4 months on the same plot). a: 3I versus BJ; b: 3I versus MET and c: BJ versus MET. In the legend. c stands for correlation and std for standard deviation.

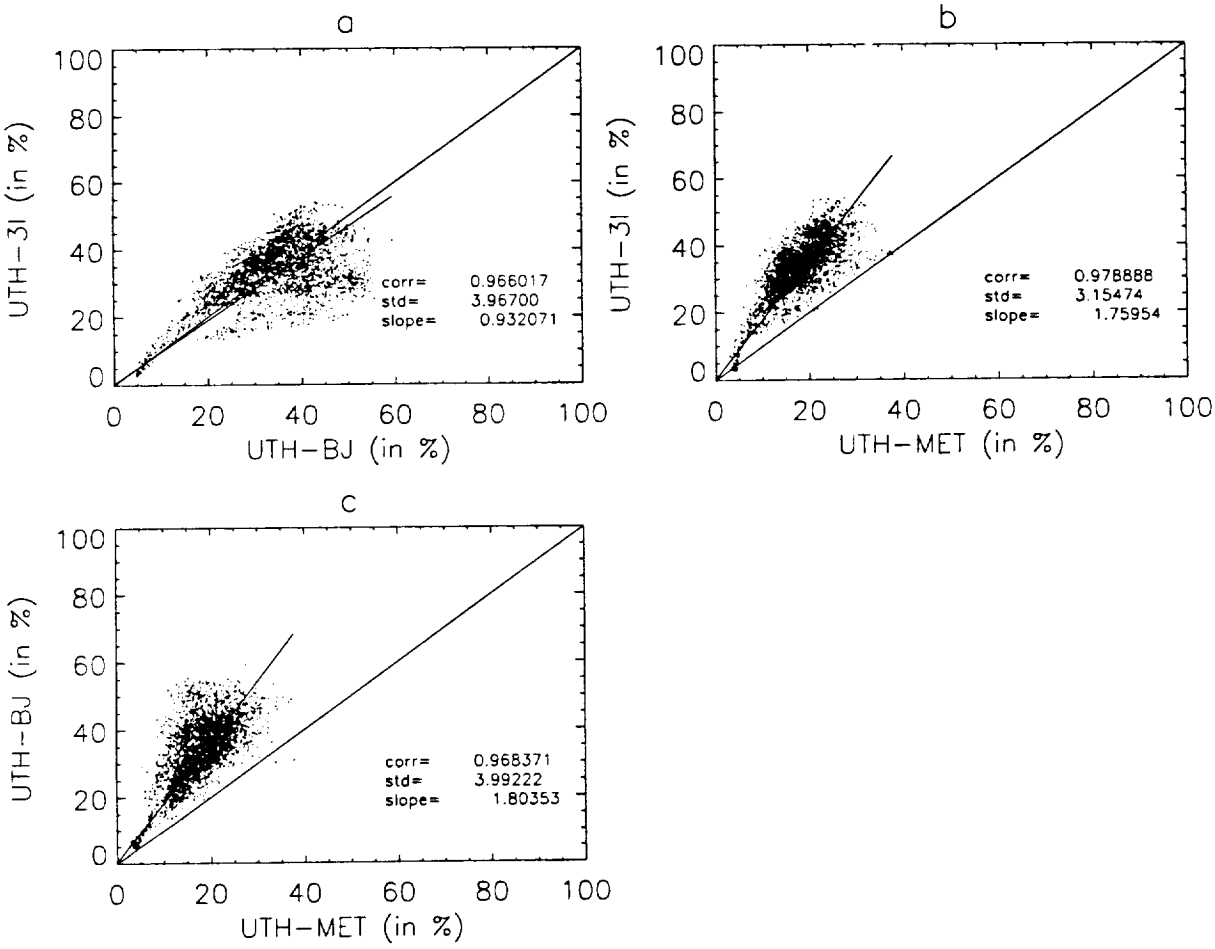


Figure 2: Same as Figure 1 in the midlatitude regions (30-60°N and 30-60°S).

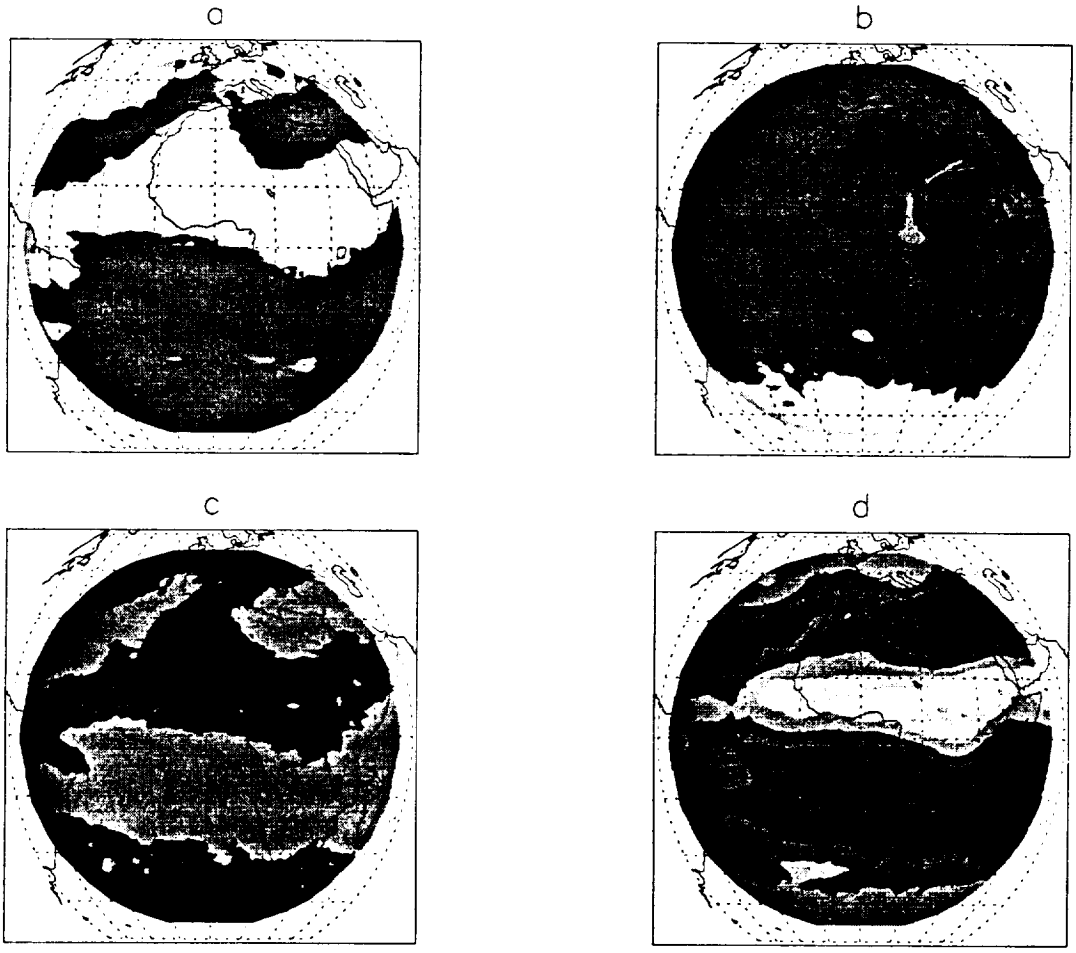


Figure 3: UTH difference (in %) between the datasets (a- 3I; b- BJ; c-MET) and the mean of the three in July. For clarity, note that light gray is between +21 and +7%; gray is between +7 and -7% and black between -7 and 21%. d: Average of the three datasets in July 1989 (in %).

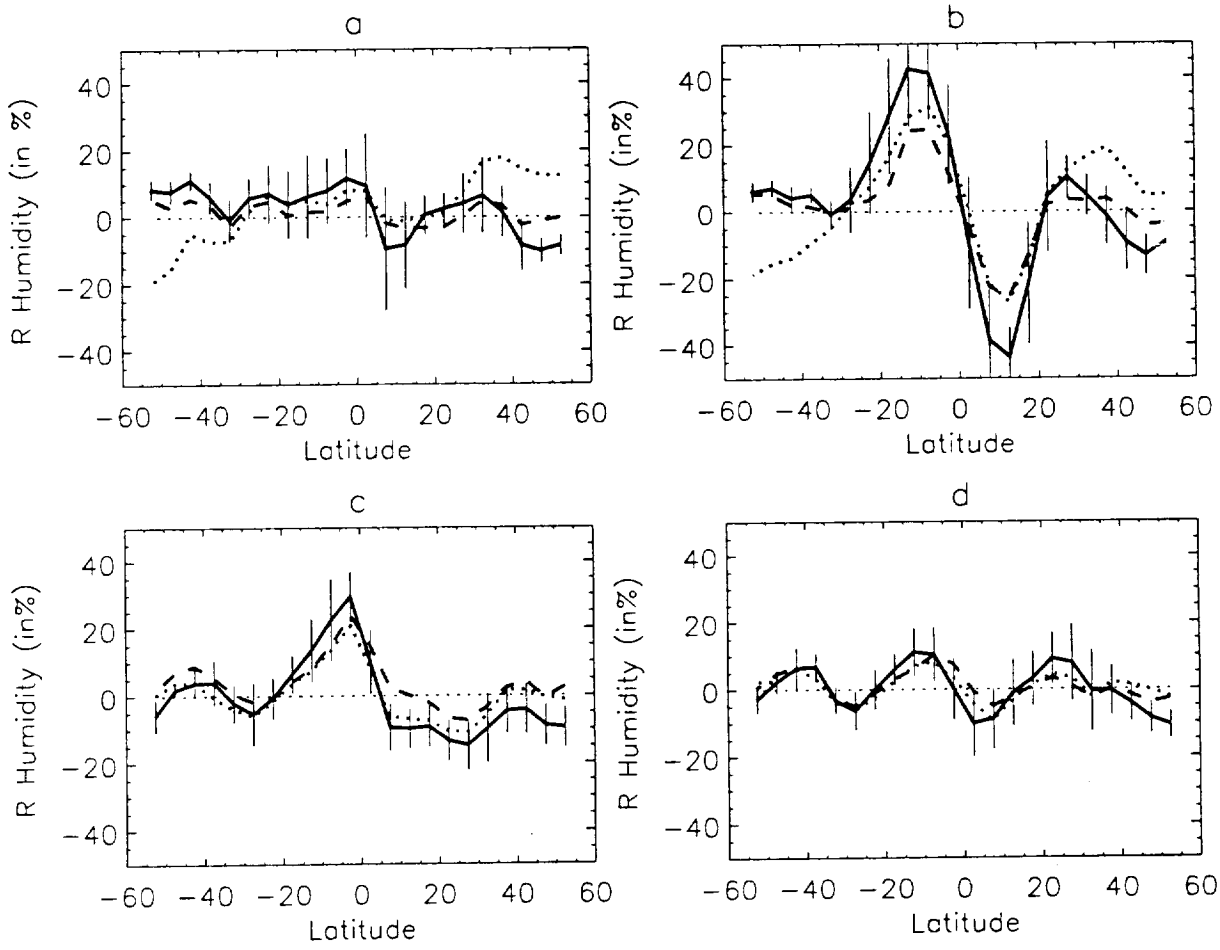


Figure 4: Monthly differences of UTH zonal mean (average on every 5° of longitude over the West part (left) and the East part (right) of the METEOSAT view). January-July difference is represented in a and b; April-October difference in c and d. Negative latitude are for southern hemisphere. The standard deviation to the zonal mean (error bar) are shown for 3I only. -3I (full line); BJ-(dotted line) and -MET (dashed dashed).

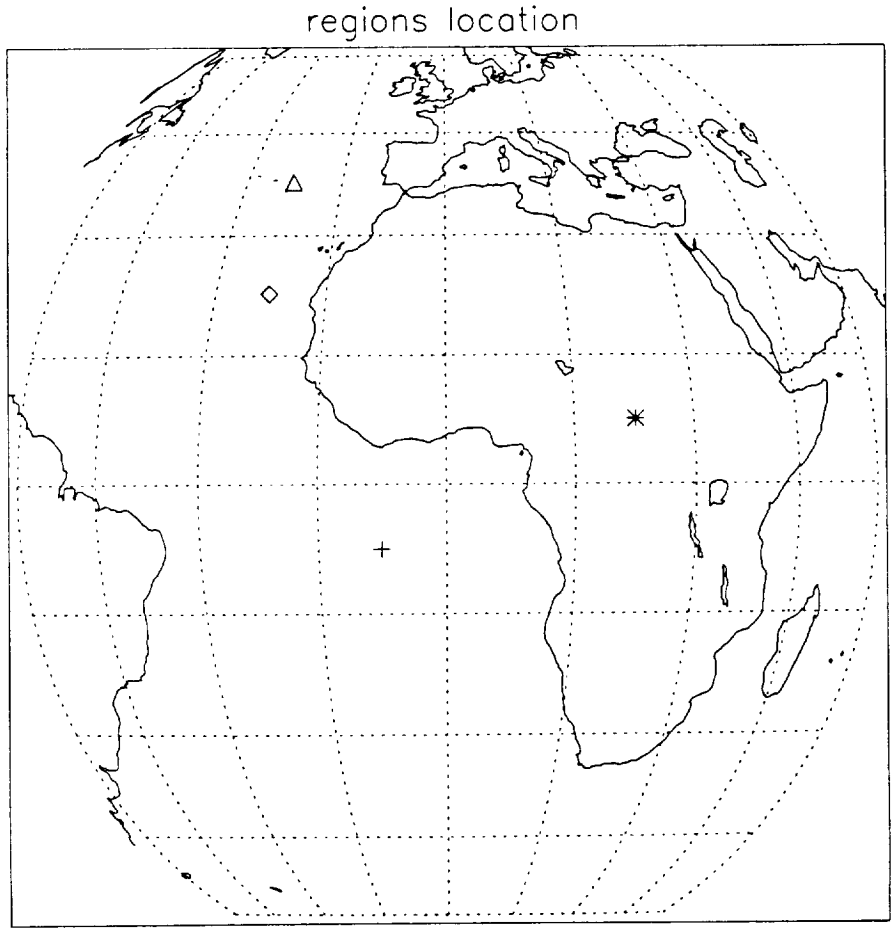


Figure 5: Position of the four selected regions [15° latitude x 15° longitude]. A is centered with a cross; B with a star; C with a diamond and D with a triangle.

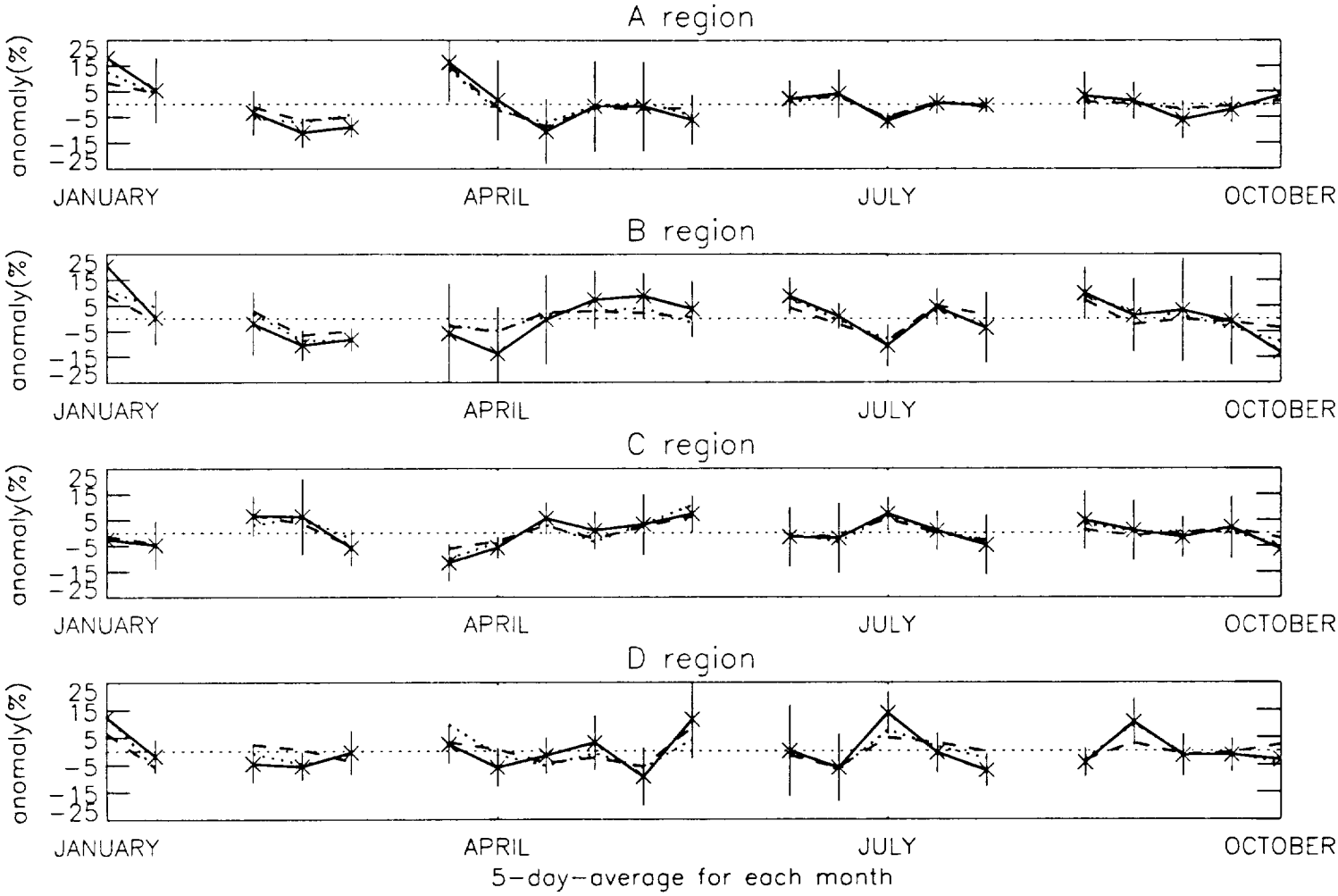


Figure 6: 5-day-average anomalies time series plotted for the four selected regions of Figure 5.

-3I (full line); -BJ (dotted line); -MET (dashed line).

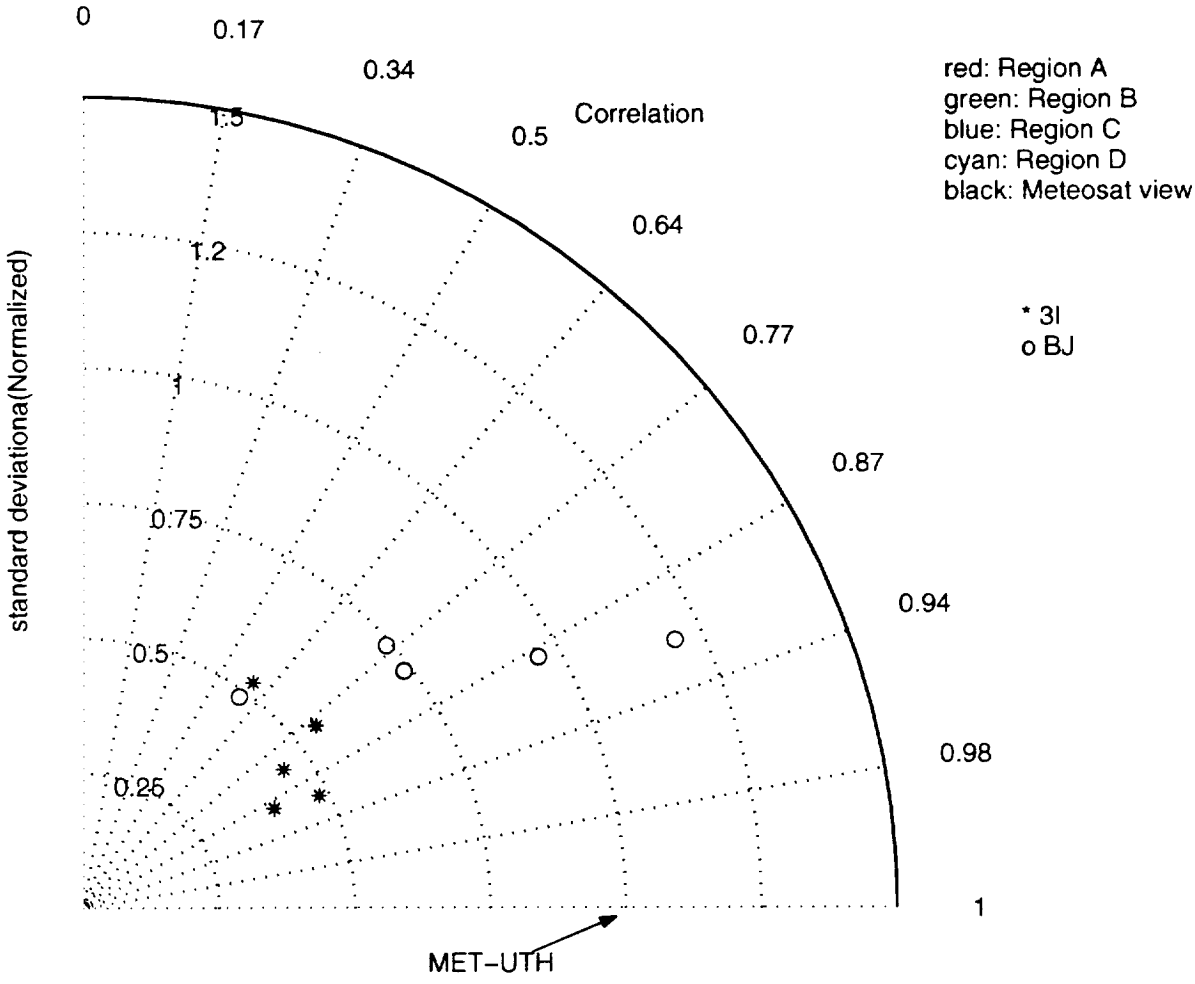


Figure 7: Taylor diagram: Space-Time variance of UTH in four regions and the global METEOSAT view by BJ and 3I with MET as reference. The radial coordinate gives the magnitude of total variance normalized to the reference dataset. and the polar coordinate gives the correlation with the reference dataset.

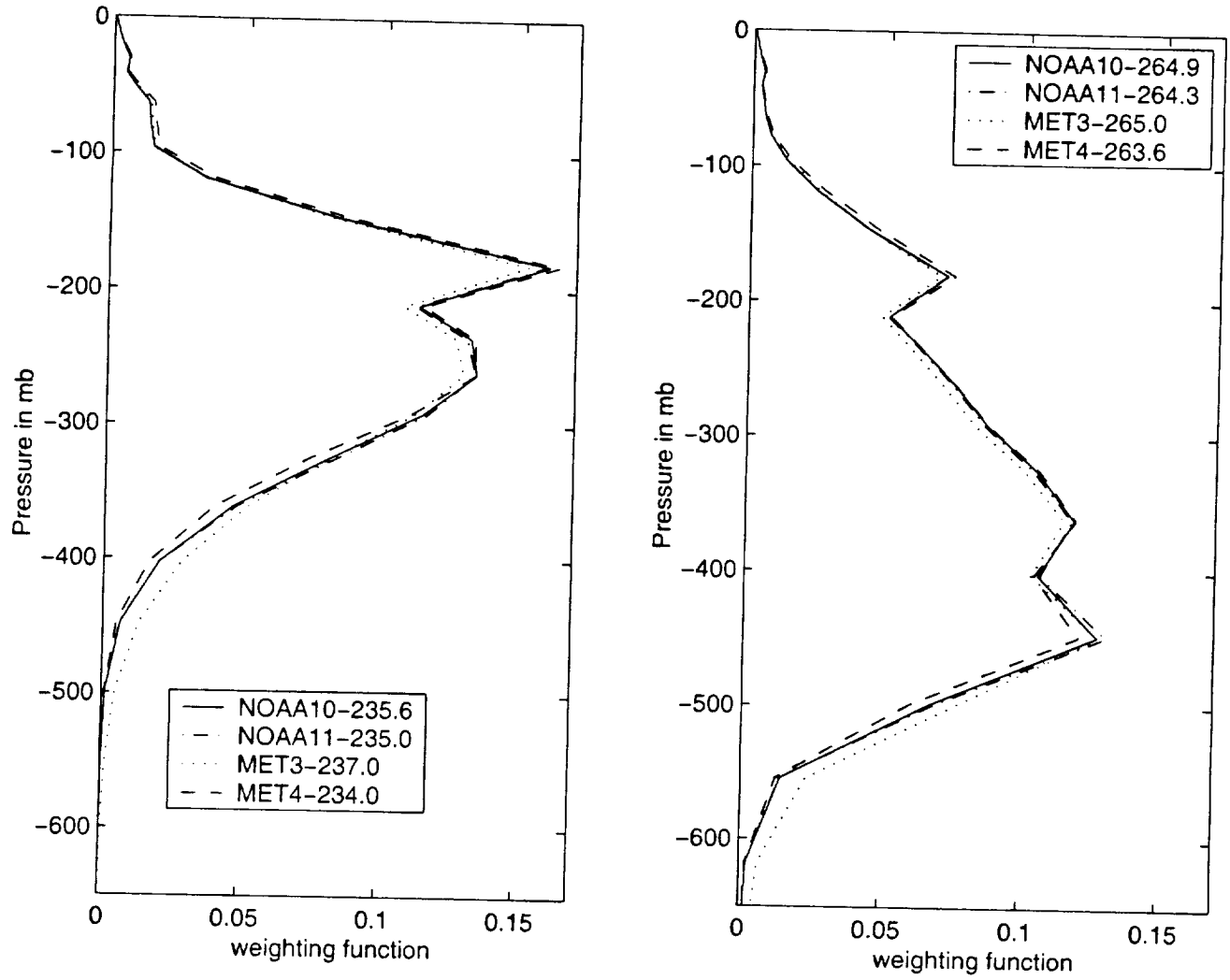


Figure 8: Water vapor channel's weighting function of four satellites (MET-3; MET-4; NOAA-10 and NOAA-11) for 2 profiles: on the left, an humid profile (300-500hPa humidity of 100%, 300-500hPa water vapor content of 1.26cm, air temperature between 246 and 270°K) and on the right, a dry profile (300-500hPa humidity of 1%, 300-500hPa water vapor content of 0.0064cm, air temperature between 235 and 263°K). In the legend, corresponding brightness temperatures follow the name of the satellite.